NAL Proposal No: 126

Correspondent: Virgil E. Barnes
Department of Physics
Purdue University
Lafayette, Ind. 47907

FTS/off-net: (317) 633-7000
749-2961

NAL BUBBLE CHAMBER PROPOSAL

Multiparticle $\pi^- p$ Interactions at 130 GeV and at the Highest Energy

Purdue High Energy Physics Group

V. E. Barnes, D. D. Carmony, R. S. Christian, E. C. Fowler, J. A. Gaidos, A. F. Garfinkel, L. J. Gutay, S. Lichtman, F. J. Loeffler, R. L. McIlwain, D. H. Miller, T. R. Palfrey, Jr., R. B. Willmann, D. Cords, J. Lamsa, K. Paler, K. Rangan, J. H. Scharenguivel.

April 23, 1971

NAL BUBBLE CHAMBER PROPOSAL

Multiparticle $\pi^- p$ Interactions at 130 GeV and at the Highest Energy

Purdue High Energy Physics Group

April 23, 1971

I. Abstract

We propose to study $\pi^- p$ (and to a lesser extent $K^- p$ and $\bar{p}p$ interactions) at 130 GeV and $\pi^- p$ interactions at the highest available energy. We use an unseparated negative beam, the NAL 30 inch bubble chamber, and a supplementary visual spectrometer consisting of wide-gap optical spark chambers with a bending magnet. Particular emphasis will be placed on quantitative studies of multiparticle final states. This will involve, among other things, a study of inclusive single particle distributions, of target and beam diffractive dissociation, and of charged particle multiplicities over a wide range of s . In addition, a scanning search in the bubble chamber for new or unusual phenomena is an important part of this proposed experiment, based on the unsurpassed usefulness of the bubble chamber in revealing outgoing charged particles and V^o's.

If proton energies approaching 500 GeV become available at the secondary hadron target, 7% $\bar{p}$ and 5% K^- are very likely to be present in the 130 GeV beam. We propose to tag them using the planned differential Cerenkov counters.

This proposal is an outgrowth of our proposals Nos. 40 and 41, submitted to NAL in June of 1970. We have added the use of a particular visual spectrometer arrangement, as have a number of groups who are submitting proposals for a coordinated set of particles and energies. The bubble chamber will be run untriggered. The spark chambers will be triggered on at most one beam track per bubble chamber picture.

We request: 200,000 pictures at 130 GeV

200,000 pictures at $p_{max} \geq 350$ GeV/c.

II. Physics Justification

1. Inclusive studies, scaling limits and multiplicity distributions.

Multiparticle events can be analyzed in the context of the parton model of Feynman, the limiting fragmentation hypothesis of Yang and co-workers, Regge theory, various multiperipheral models, the idea of pionization, and the idea of fragmentation of the target or projectile by diffractive dissociation. A number of recent studies of the process $a + b \to x +$ anything have observed apparent approach to scaling limits at existing accelerator energies.[1,2,3,4,5] Such studies should be extended over a wide range of s and to the highest possible values of s to see if the limits are really being approached, to check factorization of the distributions into separate functions of p_T and $x = 2p_L^*/\sqrt{s}$, and to check the postulated log(s) variations of the mean charged particle multiplicity $\langle n \rangle$ and the mean transverse momentum $\langle p_T \rangle$. Our two beam energies span one unit of $\ln(s)$.

Center of mass angles for fast particles can be obtained rather well from their lab. angles without knowledge of their momenta: for forward and transverse particles in the center of mass, a good approximation is that[9]

$$\log \tan \theta^* = \log \tan (\theta/2) - \log \gamma_0.$$

The bubble chamber measurements alone are useful for this determination, which relates to questions such as pionization.

2. Diffraction dissociation, missing mass spectroscopy.

Processes of the form $a + b \to a^* + b$ or $\to a + b^*$, where no exchange of Isotopic spin, charge, baryon number, G parity, or strangeness occurs, appear to be increasing or constant with beam energy at a level of roughly 0.5 mb each.[6] Will these processes still be large at 130 to 500 GeV? Double diffractive dissociation $a + b \to a^* + b^*$ is small or absent at present accelerator energies. If a^* and b^* both have masses typical of single D.D., the relatively large minimum momentum transfer at existing energies tends to suppress the process. Will the rate of double D.D. become equal to that predicted by factorization, when this restriction is removed at high energies?

In terms of studying resonances, a general feature which we expect is the opening up of very low momentum transfers to higher mass boson and nucleon resonances. Even for masses of several GeV, the minimum momentum transfer is very low, at 130 GeV, t_{min} = .01 $(GeV/c)^2$, well within the range where diffractive mechanisms are thought to be important. Since the cross section for Pomeron exchange tends to be constant, while meson exchange processes decrease as some inverse power of the beam momentum, diffractive production mechanisms may be relatively important at these energies.

Target proton dissociation can be studied in considerable detail: the decay products will be slow in the laboratory and therefore well measured. In addition, the beam pion will prefer small momentum transfer and will go through the downstream spectrometer where its momentum will be well measured.

By measuring the intermediate-range stopping recoil protons in the bubble chamber, beam pion dissociation into boson states of mass M can be studied with mass resolution[7]:

$$M = 0.26/M \text{ (GeV)}$$

for 130 GeV incident energy. This is useful for higher masses, and even allows a very crude sorting of events below 2 GeV into the general A_1 region or into higher broad mass regions.

A substantial class of events in general will have the leading proton identifiable by ionization, including also elastic events, but not including very high multiplicity events.[8]

3. Strange Particle Estimates

Slow strange particles will be produced form target dissociation into YK for example. From whatever source, if they go backward in the center of mass they will be slow in the lab. and will tend to decay in the bubble chamber, allowing an estimate of the amount of strange particle production.

Cosmic ray studies indicate a K/π ratio approaching 25%, but possibly concentrated in the proton jet, with low mass K pairs preferred[9]. We can check this, and check for anomalous N^* states involving K's or φ's. The high K/π ratio gives us further confidence in our estimate of 5% K^- in the 130 GeV beam, based on extrapolation of measurements made at Serpukhov. See the next section and Appendix.

4. $\bar{p}$ and K^- admixtures in the 130 GeV beam

If primary protons of 500 GeV/c are available, we anticipate having the first look at 7000 $\bar{p}p$ interactions and more than 2000 K^-p interactions at 130 GeV (see Appendix), as a byproduct of the main experiment. We therefore feel that mass and position tagging is very important at this energy. We will be able to obtain good quantitative information about charged particle multiplicities and inclusive distributions, and compare with the π^- data. We will be able to measure $\bar{p}p$ and K^-p absolute cross sections free of μ^- contamination. Finally, the hypercharge of both systems is $Y = 0$, which suggests the possibility of producing a wider range of strange particles than with π^-, and may increase the chance that something unusual will appear. Perhaps it is worth noting that the CERN ISR cannot study π^-p or K^-p interactions above 30 GeV.

We are submitting a separate proposal for a later experiment, with enrichment triggering of the bubble chamber flash and the fast beam kicker, when a $\bar{p}p$ or K^-p interaction occurs. If fluxes are as expected, the present experiment will lay the groundwork for the final design of the triggered experiment.

5. New, unexpected, or sought-for phenomena

The bubble chamber with its visible volume and good spatial resolution is an unrivalled tool for revealing a wide class of unanticipated phenomena. We are in an unexplored energy range where particles with a mass of 10 or 20 GeV can be produced. Heavy or backward center of mass metastable particles would have moderate or small γ factors. If the lifetimes are comparable to the known hyperons they would tend to decay within the visible volume. Their decay products would tend to be well measurable.

Produced quarks with fractional charge would be faintly ionizing relative to the incoming beam. At least two quarks must appear in any production event. Non-observation of this pattern at 500 GeV would imply either a cross section upper limit of $\leqslant 5 \times 10^{-31}$ cm^2 for quarks of mass less than 14 GeV; or else integral quark charge. If exactly two quarks were produced and if the $q\bar{q}$ system had a net charge of ± 1, the event would also contain an odd number of charged secondaries and the two faint tracks would have different ionizing powers, 1/9 and 4/9 minimum. All these configurations would be rather convincing.

Magnetic momopoles with the Dirac or Schwinger values of magnetic charge would be extremely heavily ionizing and would necessarily occur in pairs. If monopoles manifest themselves only via Ruderman-Zwanziger soft photon showers[10] an external photon detector would be needed.

We do not intend discussion of the above points to delimit the possibilities of what might be easily noticed in scanning the bubble chamber photographs. Such a scan will have our highest priority as soon as bubble chamber photographs are obtained.

III. Event Rates and Analysis Capability

Assuming ten tracks per picture and a 15" measuring fiducial volume starting at the chamber entry window, we arrive at 67,000 events per 200K pictures, or 2.7 events/μb. An equal number of events will occur in the liquid beyond the fiducial volume and a comparable number in the entrance or exit windows of the bubble chamber. Some of the non-fiducial hydrogen events whould be useful in extending the microbarn equivalent in the search for unusual phenomena.

The distribution of events among various charged prong multiplicities is shown in Table I, based upon the 200 GeV pp results from Echo Lake.[11] The exposure at maximum available energy will be similar except that the number of 14 and 16 pronged events has doubled. We have not taken account of possible differences in multiplicities when the beam is a pion.

TABLE I

Number of Charged Prongs	2	4	6	8	10	12	14	16
Number of Events	11K	17K	17K	13K	6K	3K	1.4K	.6K

Purdue will soon have an automatic measuring machine of POLLY design, capable of measuring 4000 events per week. Automatic scanning of simple event types is an early goal. We also have 7 scanning machines in operation at Purdue in Lafayette and 2 scanning machines at Purdue in Indianapolis. The group at Indianapolis has been in active collaboration with us for the past two years.

The Purdue High Energy Group consists of Professors V. E. Barnes, D. D. Carmony, R. S. Christian. E. C. Fowler, J. A. Gaidos, A. F. Garfinkel, L. J. Gutay, S. Lichtman, F. J. Loeffler, R. L. McIlwain, D. H. Miller, T. R. Palfrey, Jr., R. B. Willmann, Doctors D. Cords, J. Lamsa, K. Paler, L. Rangan, J. H. Scharenguivel and several students. In addition Professors F. T. Meiere and W. L. Yen at the Purdue-Indianapolis campus collaborate with the group.

IV. Experimental Arrangement for the Proposed 30-inch Bubble Chamber - Optical Spark Chamber Hybrid System

The main components of the proposed detector system are shown in Figure 1. These include:

(1) The 30-inch hydrogen bubble chamber, for observation of the interaction vertex and analysis of all low energy charged particles with momenta below $\sim$20 GeV/c.

(2) An upstream beam diagnostic system for providing precise measurements of beam particles.

(3) A wide gap optical spark chamber spectrometer situated downstream for providing important additional data on energetic secondary charged particles with momenta above approximately 20 GeV/c.

(4) A shower spark chamber system situated behind the spectrometer for information on very energetic gamma rays.

While the arrangement is similar in some respects to the bubble chamber - spark chamber detector system described in the Aspen study of Fields, et al.[1], it is not required for the present initial experiment to have the very high accuracy requirements for final state fitting which was of primary interest in the latter study.

These components are matched to the kinematic requirements, as discussed below, in such a way that they provide relatively complete examination of individual multiparticle interactions in the 100 GeV/c region and above. The most noticeable feature of multiparticle interactions as presently known is the tendency for the emitted particles to be produced with relatively small transverse momenta. Those going backwards in the cm system with large longitudinal momenta then appear in the laboratory system with low momenta and large angles. Particles with small longitudinal momenta can appear in the lab at intermediate momenta and angles, while the forward particles in the cm appear as highly collimated, energetic components of a forward jet.

Examples of kinematically allowed regions for transverse and longitudinal cm momenta are shown in the Peyrou plot of Figure 2 for the case of 500 GeV/c πp interactions. Superposed are the expected contours for laboratory angles and momenta of outgoing pions, showing the characteristics described above. For greater detail, the region of small transverse momenta is shown in Figure 3. Backward pions in the cm with transverse momenta below 1 GeV/c are seen to have laboratory momenta of less than $\sim$20 GeV/c, and can appear at angles even beyond 90°.

Similar behavior is illustrated for secondary protons from 200 GeV/c pp interactions in Figure 4, except that the allowed maximum laboratory angle here must be less than 90°. On the other hand, those particles produced with small or forward longitudinal momenta P_L, and transverse momenta $P_T \lesssim 1$ GeV/c, are seen to have laboratory momenta above approximately 20 GeV/c and are confined to a forward cone of less than approximately ±4° opening angle.

1. Bubble Chamber

The main bubble chamber requirements here are good track resolution, angular precision $\lesssim 1$ mrad, good momentum accuracy up to the 20 GeV/c region, and provision of suitable exit windows and magnet apertures for the forward secondaries. The 30-inch bubble chamber is eminently suitable, without requiring any significant modifications.

The gross chamber features illustrated in Figure 1 are those of the 30-inch, whose characteristics include high resolution dark field optics, a magnetic field of 32 KG, multipulsing capabilities of $\lesssim$ five expansions per 0.5 seconds, and a maximum detectable momentum of over 1000 GeV/c. In the configuration shown in Figure 1, the beam is brought in through a small window which is currently in use as an exit window for a neutral hadron hybrid spectrometer at ANL. The limiting exit angle allowed by the magnet structure in the horizontal plane is confined to approximately ±3.5°, which corresponds to allowing all secondary particles above $\sim$20 GeV/c to enter the downstream spark chamber spectrometer. In the vertical plane the magnet iron and beam exit windows allow particles at angles up to approximately ±10°. Thus, it is obvious that the analysis of tracks below $\sim$20 GeV/c will necessarily be performed in the bubble chamber, where $\Delta p/p \lesssim 10\%$ and $\Delta\theta \lesssim 1$ mrad. This, in our opinion, is a satisfactory level of performance for this particular group of produced particles.

2. Bubble Chamber Beam

Since the spectrometer facility is planned to be of general use, a comprehensive beam system is required. This section discusses beam characteristics and beam defining equipment which we regard as necessary to do a variety of experiments in the 30-inch bubble chamber with the associated downstream spectrometer. It is assumed that the beam, as described in the Lach-Pruss report[2], will be constructed, including a secondary hadron target. It is also assumed that fluxes of at least 10^{10} protons will be available at the secondary hadron target, with a spill time between 60 and 200 μ sec. Two or three such spills per accelerator pulse would be highly desirable for bubble chamber multi-pulsing. In addition, it is assumed that beam tuning detectors (scintillators or wire proportional chambers) will exist, and also at least one Cerenkov counter to determine relative fractions of π, K and p.

In addition,

A) it is felt that a flux-limiting fast kicker will permit much more efficient use of the bubble chamber, giving cleaner pictures and avoiding unusable pictures;

B) a Cerenkov counter which can efficiently tag π's vs. (K and p) up to 200 GeV/c is desirable for beam purity in view of possible significant fractions of K^- and $\bar{p}$[2,3];

C) a second Cerenkov counter which can tag (π^-, K^-) vs. $\bar{p}$ will permit studies of K^- and $\bar{p}$ interactions as a by-product of a π^- experiment. Eventually K^- and $\bar{p}$ enrichment triggering might be done. If K^+/p and π^+/p ratios are good, similar arguments will apply for positive beams;

D) position tagging of each beam track in the chamber, in time correlation with the above Cerenkov signals, will be necessary.

E) external determination of beam momentum and angles will be mandatory in most cases. Five small proportional wire chambers can do this job and also tag all beam tracks in (D).

We now discuss items (A) - (E) in greater detail.

A) <u>Fast Flux limiting Beam Kicker</u>

A 1-2 μ sec. kicker with integral Bdl $\cong$ one Kg-m would kick the 5mm high target image upward by 0.065 mrad, or by 13 mm with a 200 meter lever arm. The kicker should be located 1000 feet from the chamber. However, the beam track counter should be placed at the chamber entry window to avoid uncertainty in n. The signal propagation delay ($\sim$2 μ sec.) is comparable to the rise time, plus there are logic and ignition delays. Given a total delay of 4 to 7 μ sec., n = 10 tracks/picture, and 100 μ sec. spill time, one could control the flux to 10%, which is excellent. This is enormously better than the typical fluctuations without a kicker, and should eliminate a source of wasted bubble chamber photographs and wasted accelerator pulses.

B and C) Cerenkov Tagging of π, K and p

Extrapolations[3] of Serpukhov data indicate that 500 GeV/c protons on a target will produce a rich ratio of K^-/π^- and $\bar{p}/\pi^-$ at 100 GeV/c -- 5% and 15% respectively, 1 km. away at the bubble chamber. The need for π^- tagging in this case is obvious, and the opportunity to study tagged K^- and $\bar{p}$ interactions early is attractive. In secondary positive beams, p and π^+ and probably K^+ will all be present in significant amounts at some energies, and will require tagging.

S. Pruss (NAL) has suggested a differential Cerenkov design, an outgrowth of ideas he presented at the 1970 Summer Study[4]. Small angle light is directed to one phototube and light between this angle and a larger angle is directed to a second phototube. For Cerenkov angles $\sim$5 mrad, the angular separation of π's from K's at 200 GeV/c is several times the natural beam divergence of 10^{-4}mrad, or the chromatic $\Delta\theta$. Good photon fluxes at these angles should permit efficient tagging at p $\lesssim$ 200-250 GeV/c or beyond. A second Cerenkov counter of identical design would then permit separation of p from K and π.

The design involves 40m of Helium-filled pipe at $\sim$.2 to 1 atmosphere absolute, downstream diameter 12" to 18", a 100" focal length spherical mirror, and the above-mentioned phototube array. High counting efficiencies can be obtained even beyond 200 GeV/c in the differential mode of operation with this length. Beam divergence must be $\lesssim$ 0.1 mrad, close to what is achievable in the existing beam design.[2] Pressure must be monitored to 10 mm of mercury and average temperatures to 5°C.

D) <u>Position Tagging of Tracks to Correlate with Cerenkov Information</u>

Minimal position tagging could be accomplished with a crossed pair of picket fence scintillator arrays. This means a non-negligible number of photomultiplier tubes, since the number, m, of x-y resolution elements should be many times greater than the number, n, of beam tracks to reduce the probability of two tracks in one hodoscope location. Moreover, one must record the bubble chamber frame number and x-y for each beam track. Thus, a fast parallel shift register is needed to absorb information during the beam spill and later pass it on to a computer or perhaps directly to an incremental tape unit.

With this in mind, we suggest the use of small proportional wire arrays of 50 to 100 wires, read out as above. One gets greater x-y resolution at somewhat less cost and can also achieve the purposes of item (E). Such a system is illustrated in Figure 5.

E) <u>Angle and Momentum Tagging</u>.

To use the 30" bubble chamber efficiently, one should start the fiducial volume immediately at the beginning of the liquid. Hence, one must know p and θ of the beam externally. In any case, one can do better externally than by measuring short beam tracks in the liquid. From beam optics one will have $\delta\,\theta \simeq 10^{-4}$ rad and $\delta p/p = 0.066\%$.[2] However, in flux-limited situations one may want to increase the momentum bite to 1%. Then it pays to replace the momentum slit with a proportional wire array and win back the $\delta p/p$ inherent in the target size. This corresponds to a wire spacing of 2mm. A more refined system can be made with 1 mm. wire spacing, but several such chambers would be required to determine orbits better. In effect, the equivalent of a second plane near the target is needed to reduce the "target size". In this case one also improves upon the .066% which can be achieved with momentum slits.

The phase space of the beam as designed is 10^{-9} inch^2-steradian. With a reasonable beam size in the chamber, for example $\sim 0.5 \times 3.0$ inches, either the beam is parallel to 10^{-4} rad or its angle can be determined to 10^{-4} by measuring position in the chambers. This matches $\delta\theta_{\text{coulomb}} \lesssim 10^{-4}$ from the entry windows, and also matches for beam up to 500 GeV/c with the transverse momentum accuracy one obtains from measuring outgoing tracks in the last half of the bubble chamber or better still in the wide gap optical chambers.

To survey the proportional chambers, a well measured non-interacting track in the bubble chamber determines θ to 0.5×10^{-4} in y, and 1.5×10^{-4} in z, while $\delta\theta$(coulomb)$\sim10^{-4}$ from the entry windows. At a distance of 13 m, the wire location is known to 1.5 and 2.4 mm respectively in y and z, from a single track.

We propose to use an existing, tested design of Charpak chamber[5] with good space resolution and immunity to spark chamber noise, compact and with a relatively small number of wires in total. We could certainly put the information onto magnetic tape, together with Cerenkov counter signals, for each beam track into the bubble chamber. Frame numbers would also be written onto the tape between beam pulses. A small computer would be the most flexible readout device. A fast parallel shift register or equivalent will be needed to interface the proportional wire and Cerenkov signals. The computer could in principle be dispensed with and the information written directly from the shift register by an incremental tape unit, but with the loss of online diagnostic capabilities. Given a computer with a fast printer, the track tagging information could be printed out frame by frame for each roll, avoiding magnetic tape and associated format problems for the users.

3. Spark Chamber Spectrometer

Although many of the salient features of multiparticle interactions will be obtained from the analysis of only the low energy particles seen in the bubble chamber, as illustrated in the previous discussion, we believe that additional insight can be provided by supplementary information on the more energetic downstream components of the same events. The following deals with four important aspects of the system:

(A) spectrometer resolution,

(B) spark chamber optics,

(C) gamma-ray detection and,

(D) trigger schemes.

(A) Spark Chamber Spectrometer Resolution

The apparatus, as shown in Figure 1, includes no external magnetic field other than that of the bubble chamber itself. Calculations show that utilizing (a) the event vertex location in the bubble chamber (b) the chamber's fringing field and (c) track locations in the wide gap chambers a typical $\Delta p/p$ accuracy of ±5-10% or less is readily obtainable for fast secondaries produced in a 200 GeV/c collision on hydrogen. It is clear, however, that considerable additional accuracy is available on the very small angle fast secondaries with the addition of a magnet downstream. Preliminary considerations for such a system are also presented.

In the initial scheme, two spark chamber units are utilized, one immediately behind the bubble chamber magnet with four gaps of active volume 36" wide by 48" high by 8" deep and the other unit 4.5 meters downstream, against the far wall of the bubble chamber building, with the same dimensions. The downstream 36" dimension subtends a ±3.5° angle from the bubble chamber. Assuming the following parameters: (1) ±500 μ on each point measured in the spark chambers (2) eight points measured per spark chamber unit (3) ±50 μ on the vertex in the bubble chamber and (4) 872 KG-in of integral Bdl in the bubble chamber fringing field we find that ±Δp/p (%) $\stackrel{\sim}{-}$ 0.07 p (GeV/c). Taking into account the following sources of error due to multiple coulomb scattering: (1) 15" of LH_2 (2) 0.12" of Fe (B.C. window) (3) 0.25" of Al (vacuum tank windows) and (4) 0.5 cm of counters and other smaller sources (air, chamber walls), the resultant ±Δp/p(%) has been determined and is shown in Figure 6. With the exception of the fastest secondaries produced at the highest momenta proposed, the calculations show that the downstream spectrometer will provide data comparable in accuracy to that of the bubble chamber at lower secondary momenta and permit a complete study, in conjunction with the bubble chamber, of all interesting production angles.

The necessary and straight forward extension of the apparatus to yield more precision in the momentum determination of fast forward particles requires an additional spark chamber module plus a magnet. This would involve a large aperature magnet (e.g., an ANL type BM 109 with a 8" x 24" x 72" aperature and maximum integral Bdl of 1366 KG-in) placed immediately downstream of the second spark chamber module followed by a third spark chamber module 5 meters from the magnet. All tracks with lab momentum $\gtrsim$ 100 GeV/c and with transverse momentum $\lesssim$ 1 GeV/c will be transmitted through the aperature of the magnet and will be recorded in the third spark chamber module. The deflection in the magnet, coupled with the long lever arm, provides a ±Δp/p $\approx$ .012 p (%). Thus, 6-7% ±Δp/p or less can be achieved for all tracks of interest without altering the initial setup of the experiment.

(B) Spark Chamber Optics

The wide gap chambers have an active volume 8" deep x 48" high x 36" wide per cell. Each chamber consists of 2 cells and each module consists of 2 chambers, as seen in Figure 7. The chambers are mounted on a precision platform which has three primary functions: 1) Providing a means of determining the relative locations of the two chamber modules and the bubble chamber, 2) Providing a means of maintaining a continuous check on these positions and 3) Providing a simple means of re-installing the apparatus in the beam line after removal. Measuring of apparatus locations is done by means of two theodolites, one to determine and monitor bubble chamber-spark chamber platform positions and the second to determine and monitor spark chamber-spark chamber platform positions. Leveling legs on the chambers, top, bottom, front, and rear fiducials on the chamber frame and fiducials on the precision platform serve to position the chambers in a known orientation. Front and top fiducials also appear on each film frame to orient the chambers on the film. Rear and bottom fiducials on periodically run fiducial runs serve to complete a three dimensional co-ordinate system for track reconstruction independent of knowledge of camera position. Additional platform fiducials in view of the camera can serve as an extra check on spark chamber-platform orientations.

The chamber separation is variable within and between modules. Within the module a maximum separation of 32" is allowed. As seen in Figure 8, this maximum separation still permits viewing both chambers in a module with one 35 mm. camera at a demagnification of 64:1. This demagnification is an upper limit permitted by the intrinsic resolution of a film such as Kodak Shellburst for a real space position accuracy of 0.1 mm. With a 4" lens the camera can be located at 20 ft. from the center of the chambers. The chambers are inclined 6° relative to the beam line to permit a direct view in each chamber, thereby eliminating lenses and mirrors in that view (see Figure 9). The chamber windows are made of 10 mil. clear Mylar to eliminate distortions there. One precision mirror is used in the 90° stereo view to bring that view to the same camera. A fiducial plane with many fiducials is located at the bottom of the spark chamber to permit corrections due to any distortions in the mirror. 90° stereo is used for maximum accuracy in reconstruction. The direct view is the view of the plane of bend for maximum accuracy in momentum determination. A strip mirror subtending $\sim$ 1/3 of the gap in the direct view provides 10° stereo for resolving ambiguities in track reconstruction. The mirror subtends only part of one gap in each chamber to eliminate confusion between the direct and 10° stereo tracks. A dark room under slight over pressure surrounds each assembly for photographic and hydrogen safety reasons.

(C) Gamma-Ray Detection

The insertion of several radiation lengths of material between the second and third gaps of the spark chamber units will provide an effective converter for gamma-rays from fast, forward π^0's. From the point of interaction, probably measureable to $\lesssim$ 5 mm, both the frequency and direction of fast π^0's can be inferred. To our knowledge, the only previous measurement of π^0 frequency is that of Elbert et al.[6] at 25 GeV/c for π^-p in a hydrogen bubble chamber with plates. Their results, although somewhat weak statistically, are in rather strong disagreement with the multiperipheral model. Clearly, more precise measurements at NAL energies will be very valuable in our proposed studies.

(D) Trigger Schemes

The trigger arrangement will be designed such that the spark chambers fire on virtually all interactions, there being nearly one per beam burst. A picture of the bubble chamber will be taken for each expansion. Two simple and flexible schemes have been devised:

(1) Energy-Loss Trigger: Referring to Figure 1, multiparticle-charge-particle secondaries would be selected by pulse-height criteria in the counters S_3 S_4 S_5. More than one particle will, on the average, give a greater pulse height than that for a single beam particle. Although one might consider almost any type of counter which gives signals proportional to the number of particles which transverse it, e.g. Cerenkov, scintillation, etc., the most simple to utilize is the scintillation counter and it also turns out to result in the thinnest detector (in g/cm^2). A single scintillation counter when traversed by a high energy particle will give a Landau pulse-height distribution. This distribution, with its long tail at high pulse heights, cannot be avoided in the present application. A pulse height of 2 times the minimum value will occur on traversal by a single minimum ionizing particle $\sim$5% of the time. This can be greatly improved, however, if two or more counters S_1, S_2; S_3 $S_4 \ldots S_n$ are utilized and the minimum pulse height appearing is considered. In this case, the width of the distribution will be decreased by $1/\sqrt{n}$ and even for n = 3, the tail has all but vanished. If this signal is to be used to trigger the downstream chambers, the minimum pulse height must be determined in <<1 μ sec.

With this method, it is to be noted that the downstream counters should be thin in order that nuclear interactions in them do not occur frequently. Such interactions are no different in character from those in the chamber and walls and triggers due to them would certainly result. The number of these should be much smaller than those which occur in the chamber. In 1 mm of plastic scintillator a minimum ionizing particle produces $\sim 10^3$ photons. With an efficient photo cathode ($\sim$25%) and a light collection efficiency of $\sim$20%, 50 photo-electrons could result. This number is sufficient to assure that statistical fluxtuations will be relatively small. The five counters, S_1, S_2, S_3, S_4, and S_5, would represent a total thickness of 0.5 cm which is 0.5cm/52cm = 1/100 of a geometrical-mean-free-path. Thus, with 6 particles per picture and with the counters described, in $\sim$ 6% of the pulses would the spark chamber system have recorded interactions occuring in the triggering counters $S_1S_2S_3S_4$and S_5.

For reasons of efficient and uniform light collection the size of these counters probably should not exceed 8" x 8". This presents some minor limitations in the detection of secondaries as they must appear within a cone of ±3° if placed at a distance of $\sim$2 meters from the interaction. It may be possible to locate counters nearer the chamber inside the iron yoke, and if so the acceptance angle would be increased. This setup is very inefficient for elastic scattering and processes of the type $pp \rightarrow ppn(\pi^\circ)$, when the struck proton is slow and at a large angle, thus missing $S_3S_4S_5$. However, an alternate scheme, discussed next, would resolve this shortcoming. Also, with this arrangment one also might consider triggering on events with no charged secondary within the angular acceptance of $S_3S_4$and S_5. This alternate trigger could be tried with parallel logic and could be easily included or not as a parallel trigger.

(2) Beam-Deflection Trigger: The trigger consists of a 3.0 inch diameter scintillator S_3 located in the beam 125 feet downstream from the

bubble chamber (see Figure 1). When this scintillator fails to record a particle previously observed by counters S_1, S_2 in the beam upstream of the bubble chamber, it is considered to have interacted.

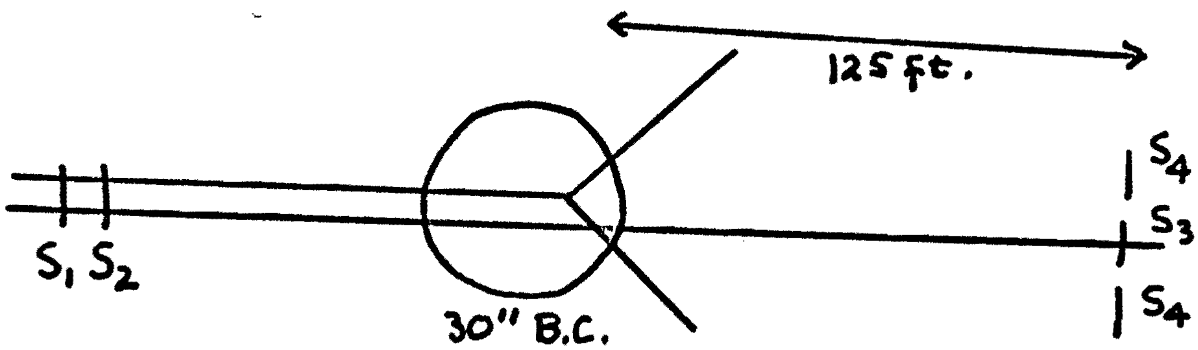

For the purposes of investigating the properties of the trigger we assume a 2.0" diameter beam in the bubble chamber. This allows a beam spread which does not diverge after leaving the chamber except for multiple Coulomb scattering. For beam momenta between 100 and 500 GeV/c the beam size at the downstream scintillator should not exceed 2.25 inches due to multiple scattering.

This trigger fails most frequently in detecting elastic scatters. Table II below lists the average minimum scatter angle and recoil range for elastic events which will actuate the trigger.

TABLE II - Minimum Angle and Recoil Range For Elastic Events

Beam Momentum GeV/c	Minimum Scatter Angle mr.	Minimum Recoil Range cm
100	1	0.3
200	1	3.5
300	1	15.0
500	1	100

There is considerable flexibility here. For example, by moving S_3 to 200 feet downstream of the bubble chamber and using a diameter of 2.5" instead of 3.0", one achieves a minimum angle of 0.5 mr. and a minimum range of 8.0 cm at 500 GeV/c.

Some fraction of the inelastic events might also be expected to put a particle through S_3, invalidating the trigger. Scaling 25 GeV/c events to NAL energies indicates this is not very important, in part because the bubble chamber field imparts transverse momentum to a track which is several times that of the minimum detectable elastic scatter. For example at 200 GeV/c this trigger fails on 4.5% of the 2-prongs, 3% of the 4-prongs, 1% of the 6-prongs and 0.3% of the 8-prongs.

This small loss of inelastic events can be reduced somewhat by surrounding S_3 with a larger counter S_4. A hole in S_4 passes beam particles on to S_3. A multiparticle accidental through S_3 is likely to be accompanied by one or more particles through S_4. Hence one would trigger on $(S_1.S_2.\overline{S_3}.S_4)$, $(S_1.S_2.\overline{S_3}.\overline{S_4})$, $(S_1.S_2.S_3.S_4)$. One can reduce the loss rate arbitrarily by increasing the size of S_4 or moving it closer to the bubble chamber.

S_3 was not placed more than 125 feet downstream of the bubble chamber so that transit time of the particles and signals would be short enough to allow adequate time to perform logical operations and apply spark chamber voltages in less than 500 ns. This restriction is probably too strict by at least a factor of two and can probably be relaxed to observe smaller angle elastic scatters. Some groups will probably prefer a beam profile in the chamber more like 5" x 1/2". In this case S_3 would be about 6.5" x 1". This has approximately the same solid angle as the circular counter discussed above and presents no focusing problems for the presently planned beam.

Finally, it is emphasized that both these triggers are flexible and most certainly can be studied quickly and efficiently under test beam conditions. It would be our intention to do so before proceeding with "production" data-taking.

REFERENCES (SECTIONS I-III)

1. R. W. Anthony et al., Phys. Rev. Lett. 26, 38 (1971).
2. Benecke, Chou, Yang and Yen, Phys. Rev. 188, 2159 (1970).
3. J. C. Vander Velde, Phys. Lett. 32B, 501 (1970).
4. Bali, Brown, Peccei and Pignotti, Phys. Rev. Lett. 25, 557 (1970).
5. Chan, Wang and Wong, Phys. Rev. Lett. 26, 280 (1971).
6. W. Walker, p. 295, "High Energy Collisions", Stony Brook (Gordon and Breach, 1969).
7. D. H. Miller, NAL SS69, Vol. 2, p.35.
8. A. Erwin, Conference on Expectations for Particle Reactions at the New Accelerators (Wisconsin, March 1970).
9. M. Koshiba, p.161, "High Energy Collisions", Stony Brook (Gordon and Breach, 1969).
10. M. Ruderman and D. Zwanziger, Phys. Rev. Lett. 22, 146 (1969).
11. L. W. Jones et al., Phys. Rev. Lett. 25, 1679 (1970).

REFERENCES (SECTION IV)

1. T. H. Fields, et al., NAL Summer Study, Vol. 3, 227 (1968).
2. "Hadron Beams in the neutrino Area", J. Lach and S. Pruss, NAL Report TM-285, 2254.000.
3. "Extrapolated Ratios of K^- and $\bar{p}$ to π^- from High Energy Protons on Aluminum measured at Serpukhov," V. E. Barnes, Purdue University High Energy Physics Note # 313, April 1, 1971.
4. S. Pruss, NAL Summer Study (1970) p. 103.
5. M. Atac and J. Lach, Nucl. Instr. & Methods 86, (1970) p. 173.
6. J. W. Elbert et al., Nuclear Physics B19, 85 (1970).

FIGURE CAPTIONS

Fig. 1 Components of the proposed hybrid system.

Fig. 2 Contours of laboratory angle and momentum on the Peyrou Plot for the π in the reaction $p + p \rightarrow \pi^{+} + \ldots$ at 500 GeV/c.

Fig. 3 Shows more detail of Fig. 2.

Fig. 4 Detail of contours of laboratory angle and momentum on the Peyrou Plot for the proton in the reaction $p + p \rightarrow p + \ldots$ at 200 GeV/c.

Fig. 5 Upstream proportional wire spectrometer.

Fig. 6 Calculated momentum resolution for the apparatus of Fig. 1.

Fig. 7 Wide gap optical spark chamber (one of two such chambers).

Fig. 8 Wide gap optical spark chambers and camera positioning.

Fig. 9 Format of images on 35 mm film.

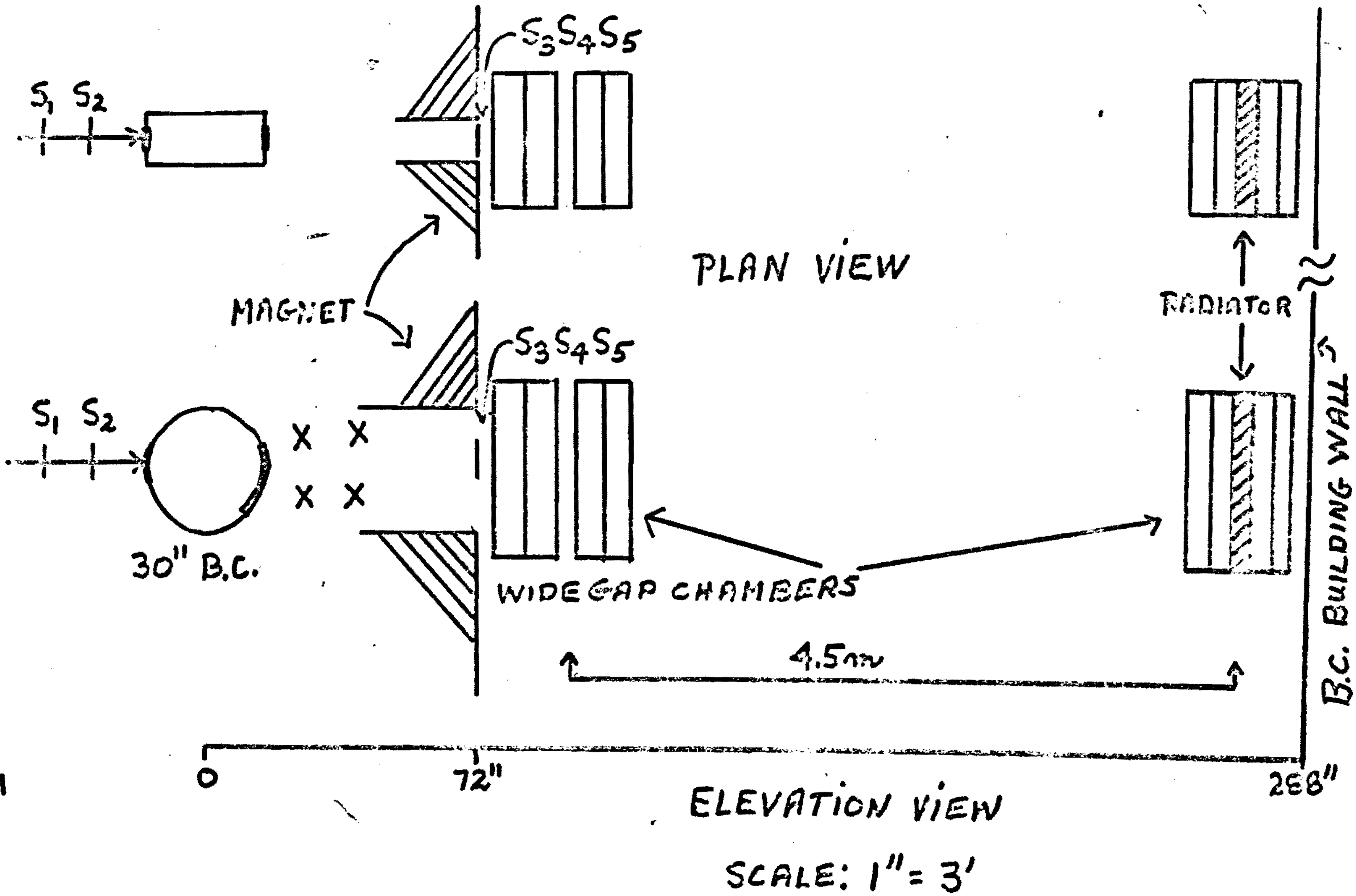
S_1 S_2
$S_3 S_4 S_5$
PLAN VIEW
MAGNET
RADIATOR
S_1 S_2
$S_3 S_4 S_5$
30" B.C.
WIDE GAP CHAMBERS
4.5m
B.C. BUILDING WALL
0
72"
288"
ELEVATION VIEW
SCALE: 1" = 3'

Figure 1

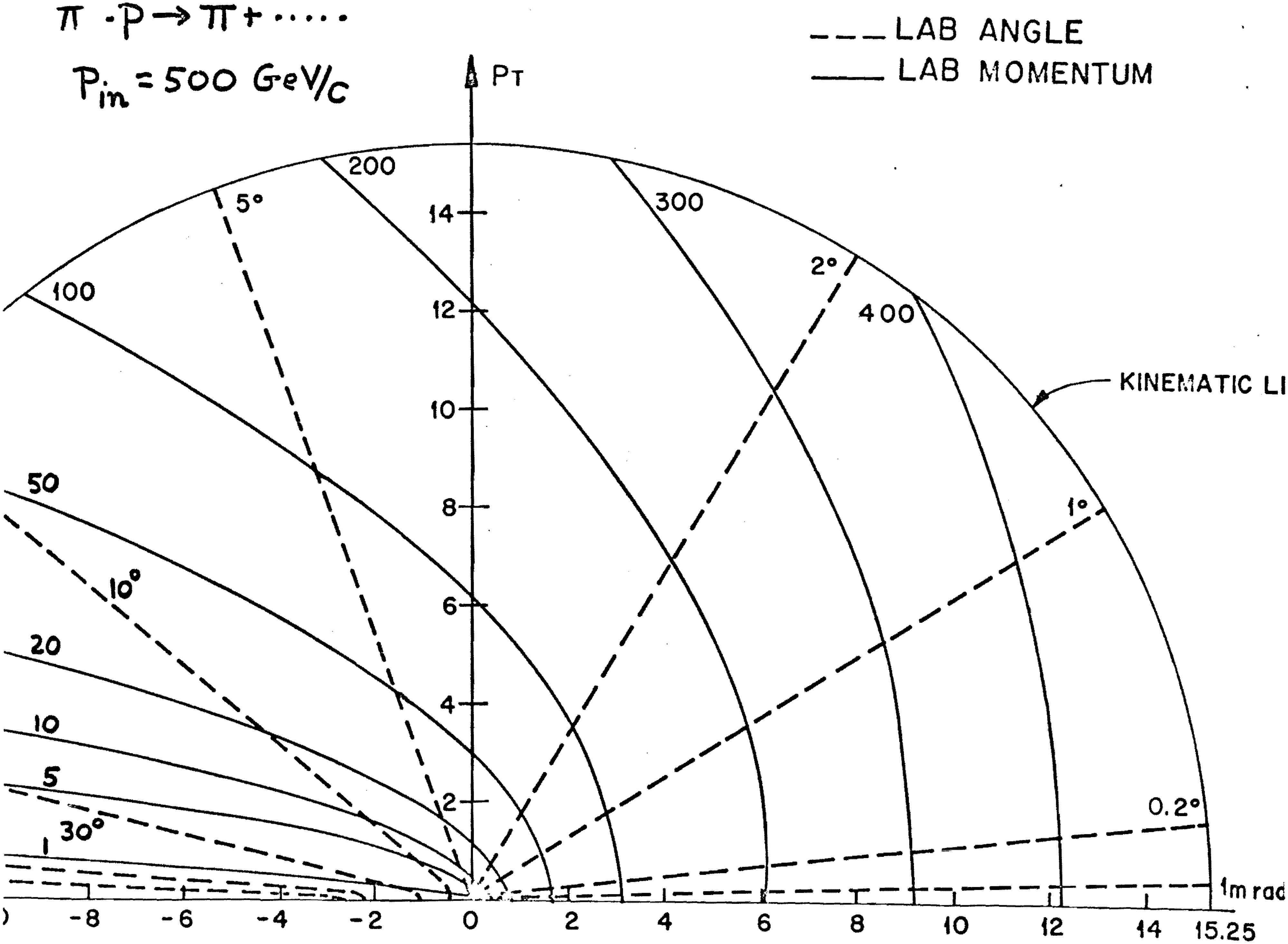
π · P → π + ...
P_{in} = 500 GeV/c
LAB ANGLE
LAB MOMENTUM
PT
PL
KINEMATIC LIM
100
200
300
400
50
20
10
5
1
5°
2°
1°
10°
30°
0.2°
1m rad
14
12
10
8
6
4
2
-8
-6
-4
-2
0
2
4
6
8
10
12
14
15.25

FIG. 2

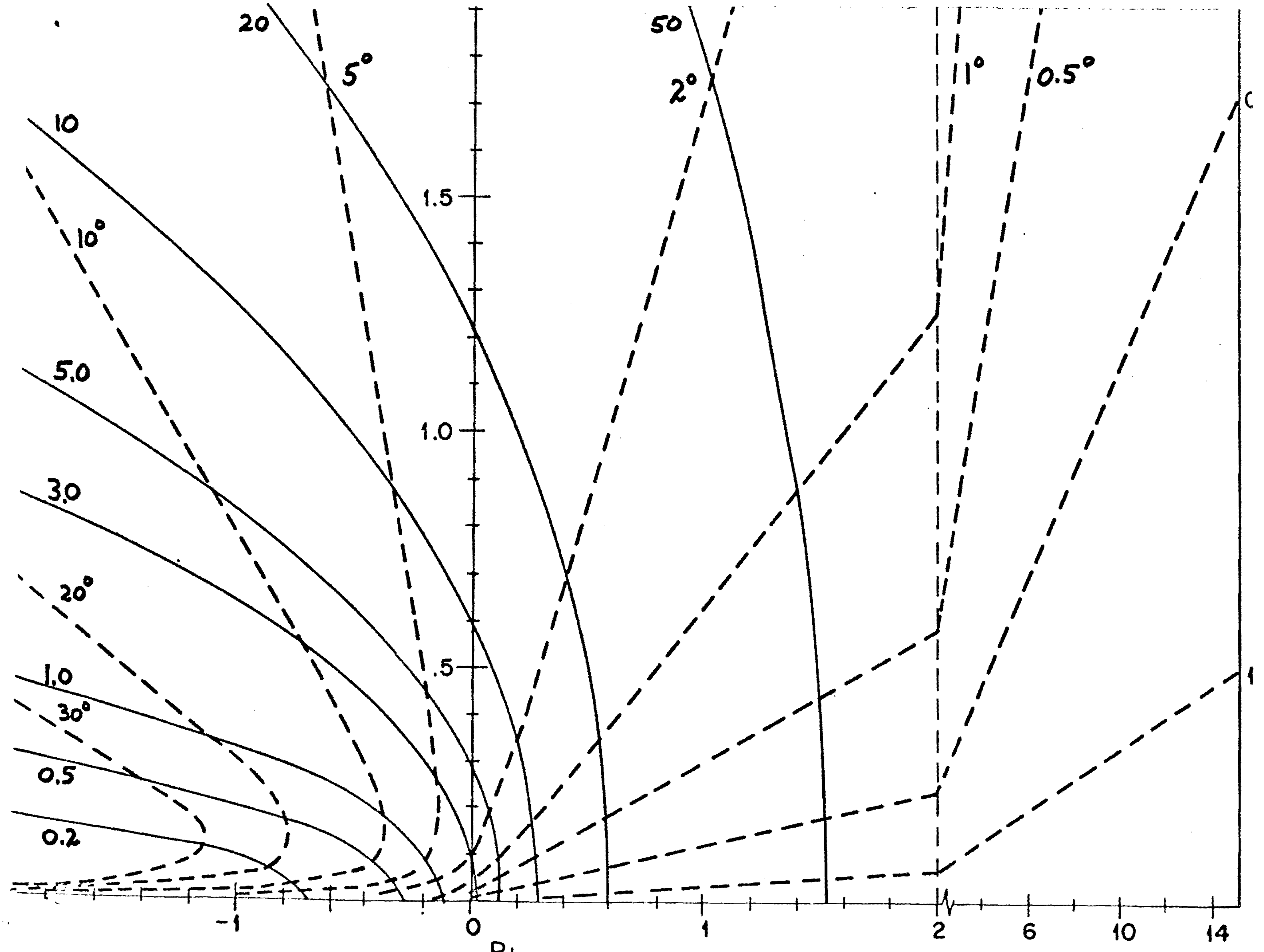

FIG. 3

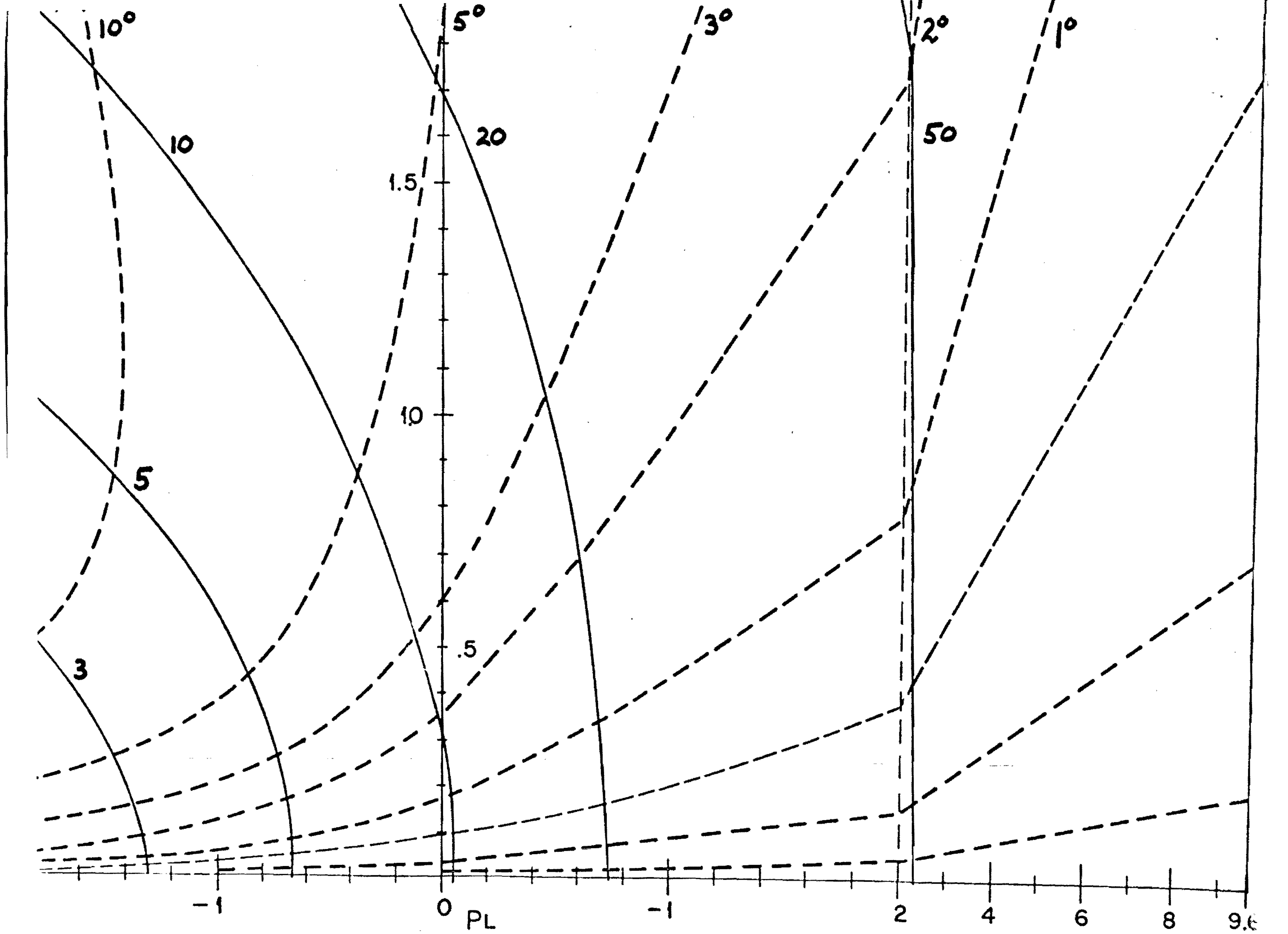

FIG.4

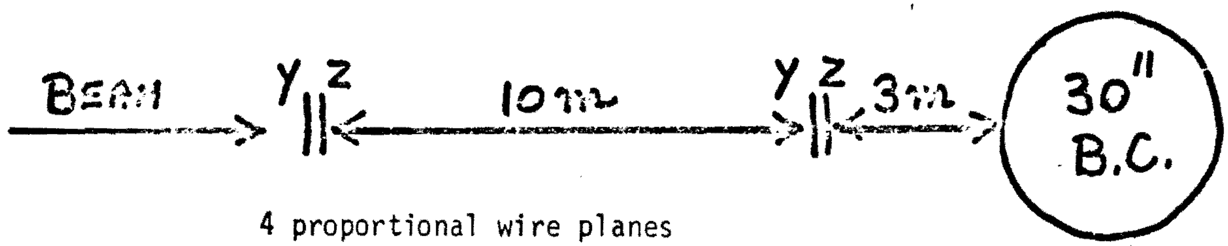

4 proportional wire planes

1 mm wire spacing

2"x2", 50 wires. This can be scaled up by a factor 2 in y if needed.

The momentum defining proportional chamber is not shown, being over 1000' upstream at a focus where the image of the target is ~2 mm in size. The dispersion is ~2 "/% at this point.

FIGURE 5

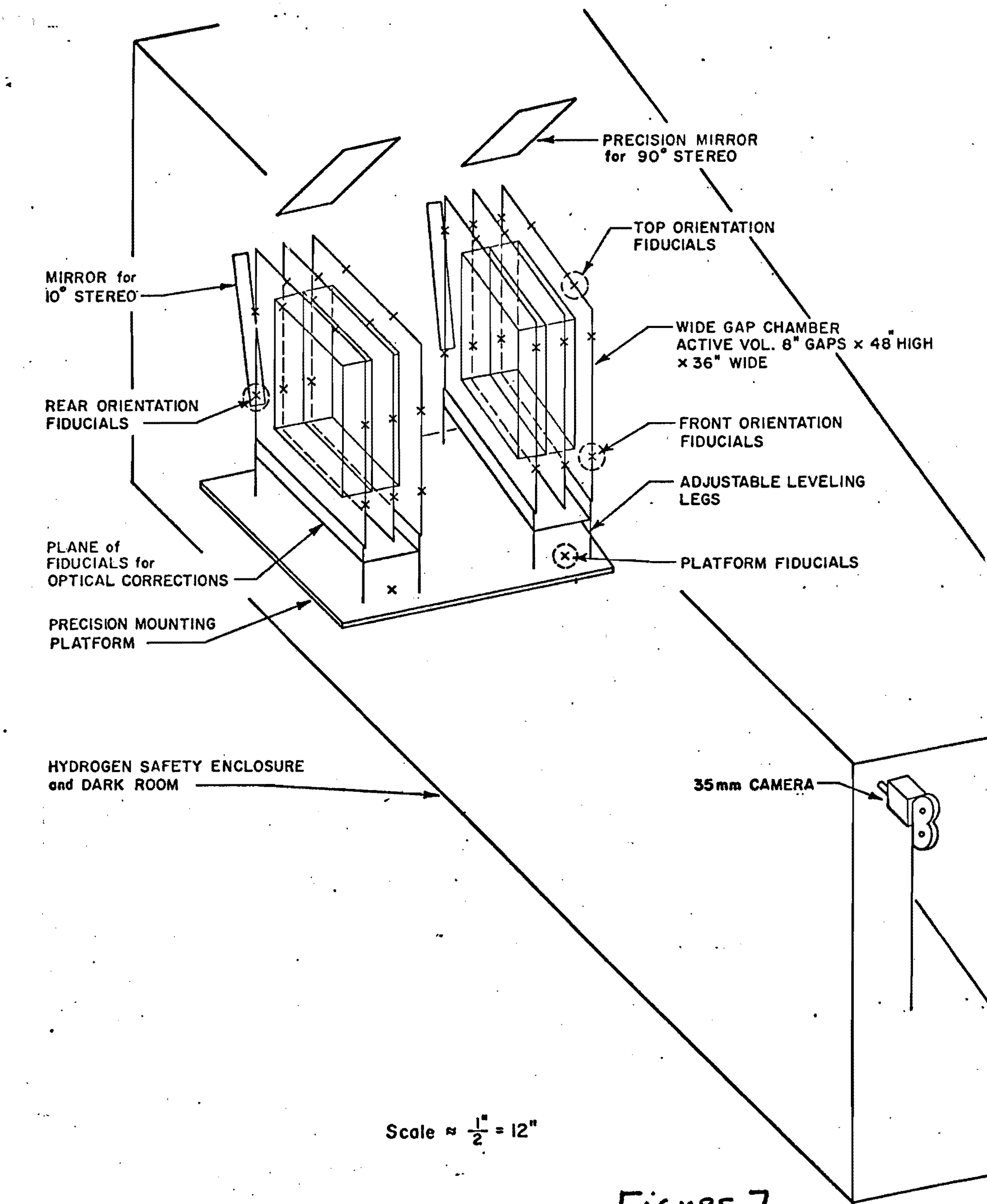
PRECISION MIRROR for 90° STEREO
TOP ORIENTATION FIDUCIALS
MIRROR for 10° STEREO
WIDE GAP CHAMBER ACTIVE VOL. 8" GAPS × 48" HIGH × 36" WIDE
REAR ORIENTATION FIDUCIALS
FRONT ORIENTATION FIDUCIALS
ADJUSTABLE LEVELING LEGS
PLANE of FIDUCIALS for OPTICAL CORRECTIONS
PLATFORM FIDUCIALS
PRECISION MOUNTING PLATFORM
HYDROGEN SAFETY ENCLOSURE and DARK ROOM
35mm CAMERA
Scale ≈ 1"/2 = 12"

FIGURE 7

SUBJECT K^- and $\bar{p}$ Fluxes in the 1000 Meter Hadron Beam and Event Rates in the 30" Bubble Chamber.

NAME Virgil E. Barnes

DATE April 21, 1971

APPENDIX I.

Serpukhov data published in Physics Letters indicate that $\bar{p}$ and K^- as a fraction of π^- are increasing with bombarding energy,[1] at a fixed value of p_-/p_{max} where p_- is the outgoing K^- or $\bar{p}$ laboratory momentum and p_{max} is roughly the bombarding momentum. Also, these fractions increase as p_-/p_{max} becomes smaller. More recent Serpukhov data[2] at 70 GeV, which go to lower values of p_-/p_{max}, show that the richest ratios occur for $p_-/p_{max} = 0.2$. The table on the following page is for $p_-/p_{max} = 0.2$ and 0.4. Due to substantial K^- decay over the 1000 meter beam length, the ratio $R(K^-)$ is roughly a constant 5% over this range of p/p_{max}, when the bombarding energy is 500 GeV.

For out choice of a 130 GeV secondary beam ($p/p_{max} = 0.26$) using the methods outlined on the next page we have at the bubble chamber:[3]

$P_{\text{primary proton}}$	500 GeV	200 GeV
K^-/π^-	4.7%	1.4%
$\bar{p}/\pi^-$	6.7%	0.4%

We base our event rates on a 15" fiducial volume, 10 Hadron tracks per picture, and a 200,000 picture exposure, giving 2.74 events/μb. We estimate $\sigma(\pi^- p) = 24.5$ mb, $\sigma(K^- p) = 21$ mb, and $\sigma(\bar{p}p) = 42$ mb above 100 GeV, equal to the measured Serpukhov cross sections at around 60 GeV.

130 GeV/c Interactions	P_{proton} = 500 GeV/c	P_{proton} = 200 GeV/c
$\pi^- p$	61,000 events	67,000 events
$K^- p$	2,400	800
$\bar{p}\,p$	6,800	460

We expect K^- and $\bar{p}$ to be negligible when the momentum is near p_{max}.

REFERENCES

1. F. Binon et al., Phys. Lett. 30B, 506 (1969).
2. Yu M. Antipov et al., Phys. Lett. 34B, 164 (1971)
3. The ~~meson~~ Muon contamination is expected to be small. See Appendix II.

SUBJECT

NAME V. E. Barnes

DATE April 1, 1971

APPENDIX

Extrapolated Ratios of K^- and $\bar{p}$ to π^-, from High Energy Protons on Aluminum, measured at Serpukhov.

Figure 1 suggests that $R(K^-)$ and $R(\bar{p})$, defined as fractions of outgoing π^-, increase with proton bombarding energy from 19 to 78 GeV for a fixed value of P_K-/P_{max} or $P_{\bar{p}}/P_{max}$.

Figure 2 shows this variation, for $P-/P_{max} = 0.4$. Both R's seem to increase logarithmically with $P_{inc.}$, and have been so extrapolated. Similar trends obtain for $P-/P_{max} = 0.5$ and 0.6.

Figure 3 extends the "universal" shape of Figure 1 down to $P-/P_{max} = 0.1$ and shows that the R's peak when $P-/P_{max} \sim 0.2$. $R(K^-)$ increases by a factor ~1.8 and $R(\bar{p})$ increases by a factor ~5 when $P-/P_{max}$ goes from 0.4 to 0.2 (at $P_{inc.}$ = 70 Gev/c).

We thus estimate the following ratios. Decays of π^- and K^- over a 1,000 meter beam length are taken from Table I. $R(K^-)$ suffers; but $R(\bar{p})$ improves from decay of π^-.

500 GeV p on Al.		% of π^-	1000m, % of π^-	200 GeV p on Al		% of π^-	1000m, % of π^-
100 GeV	K^-	18%	5.6%	40 GeV	K^-	14%	0.77%
200 GeV	K^-	8%	4.5%	80 GeV	K^-	8%	1.85%
100 GeV	$\bar{p}$	13%	15.5%	40 GeV	$\bar{p}$	10%	15.60%
200 GeV	$\bar{p}$	2%	2.2%	80 GeV	$\bar{p}$	2%	2.50%

Hagedorn-Ranft calculations also indicate ratios about like this at production angles of 5 to 10 mrad, while at 0^o production the Hagedorn-Ranft ratios are considerably smaller, as in the figures of the NAL report on Hadron Beams to the Bubble Chambers, by J. Lach and S. Pruss, TM-285 2254.000

APPENDIX I

TABLE I

1000 Meter Beam, K^- and π^- Decays

P^- (GeV/c)	30	40	50	80	100	120	150	200	300	400	500
K^-, % Remaining	1.1	3.5	7.3	18.5	26	32	41	51	64	72	77
π^-, % Remaining	55	64	70	80	84	90	91	91.5	94	95.5	97.5
R_D decay ratio K^-/π^-	0.02	0.055	0.104	0.23	0.31	0.36	0.45	0.56	0.68	0.76	0.79

$\beta\gamma = P/m$	$c\tau_{K^-} = 3.7$ m	$\beta\gamma c\tau = p(\text{GeV}) \times 7.4$	$N/N_o = e^{-L/7.4p} = e^{\frac{-135}{p}}$
$N = N_o\, e^{-(L/\beta\gamma c\tau)}$			
$L = 1000$ m	$c\tau_{\pi^-} = 7.81$ m	$\beta\gamma c\tau_{\pi^-} = p(\text{GeV}) \times 55.8$	$N/N_o = e^{-L/55.8P} = e^{\frac{-18}{P}}$

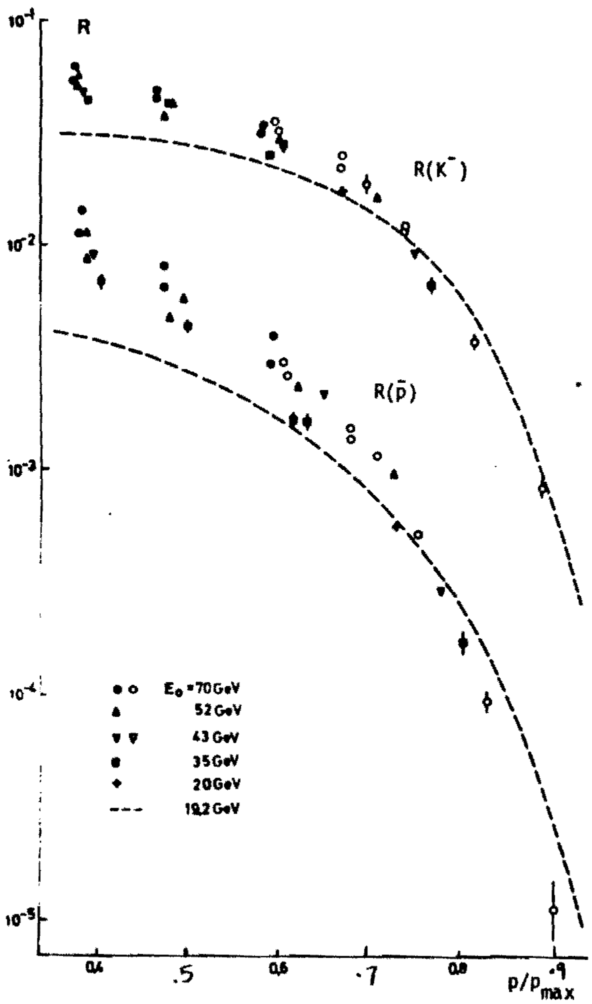

Fig. 3. Production ratios R as a function of p/p_{max}. The broken curves refer to p-p collisions [4] at 19.2 GeV.

is observed for the ratio $R(K^-)$ but it is somewhat less pronounced.

The differential cross-sections for the production of particles were obtained by a method already described [1]. The computed beam luminosity $\Delta\Omega \cdot \Delta p$ was used for their evaluation. The computed value of Δp, the momentum acceptance, has been checked in a measurement made with the differential Čerenkov counter. The relative flux of protons hitting the aluminium target was deduced from the measurement of the induced ^{22}Na activity. Absolute values of the cross-sections have been obtained by normalizing the data with the 40 GeV/c value [1].

The differential cross-sections for π^- production in aluminium by 70 GeV/c protons are given in table 1. The flux of π^- keeps increasing quickly as momentum decreases down to 25 GeV/c. It is multiplied by a factor of 3 by going from 40 GeV/c to 25 GeV/c.

In the region of low momentum at the IHEP synchrotron, it should be possible to obtain intense beams of antiprotons. Already, at a momentum of 25 GeV/c, for a 1 GeV/c momentum bite, the flux of antiprotons is larger than 10^4 per burst.

References

1. Yu. B. Bushnin, S. P. Denisov, S. V. Donskov, A. F. Dunaitsev, Yu. P. Gorin, V. A. Kachanov, Yu. S. Khodirev, V. I. Kotov, V. M. Kutyin, A. I. Petrukhin, Yu. D. Prokoshkin, E. A. Razuvaev, R. S. Shuvalov and D. A. Stoyanova, J. V. Allaby, F. Binon, A. N. Diddens, P. Duteil, G. Giacomelli, R. Meunier, J.-P. Peigneux, K. Schlupmann, M. Spighel, C. A. Stählbrandt, J.-P. Stroot and A. M. Wetherell, Preprint IHEP 69-18 (1969), Phys. Letters 29B (1969) 48.
2. F. Binon, S. P. Denisov, P. Duteil, V. A. Kachanov, V. M. Kutyin, Yu. D. Prokoshkin, E. A. Razuvaev, R. S. Shuvalov, M. Spighel and J.-P. Stroot, Int. Conf. on Elementary particles, Lund, 1969.
3. J. V. Allaby, Yu. B. Bushnin, S. P. Denisov, A. N. Diddens, R. W. Dobinson, S. V. Donskov, G. Giacomelli, Yu. P. Gorin, A. Klovning, A. I. Petrukhin, Yu. D. Prokoshkin, R. S. Shuvalov, C. A. Stählbrandt and D. A. Stoyanova, Int. Conf. on Elementary particles, Lund, 1969, Phys. Letters 30B (1969) 500.
4. J. V. Allaby, F. Binon, A. N. Diddens, P. Duteil, A. Klovning, R. Meunier, J.-P. Peigneux, E. L. Sacharidis, K. Schlupmann, M. Spighel, J.-P. Stroot, A. M. Thorndike and A. M. Wetherell, Paper submitted to the 14th Int. Conf. on High-energy physics, Vienna (1968) (CERN, Geneva, 1968).

* * * * *

FIGURE 1

Appendix I

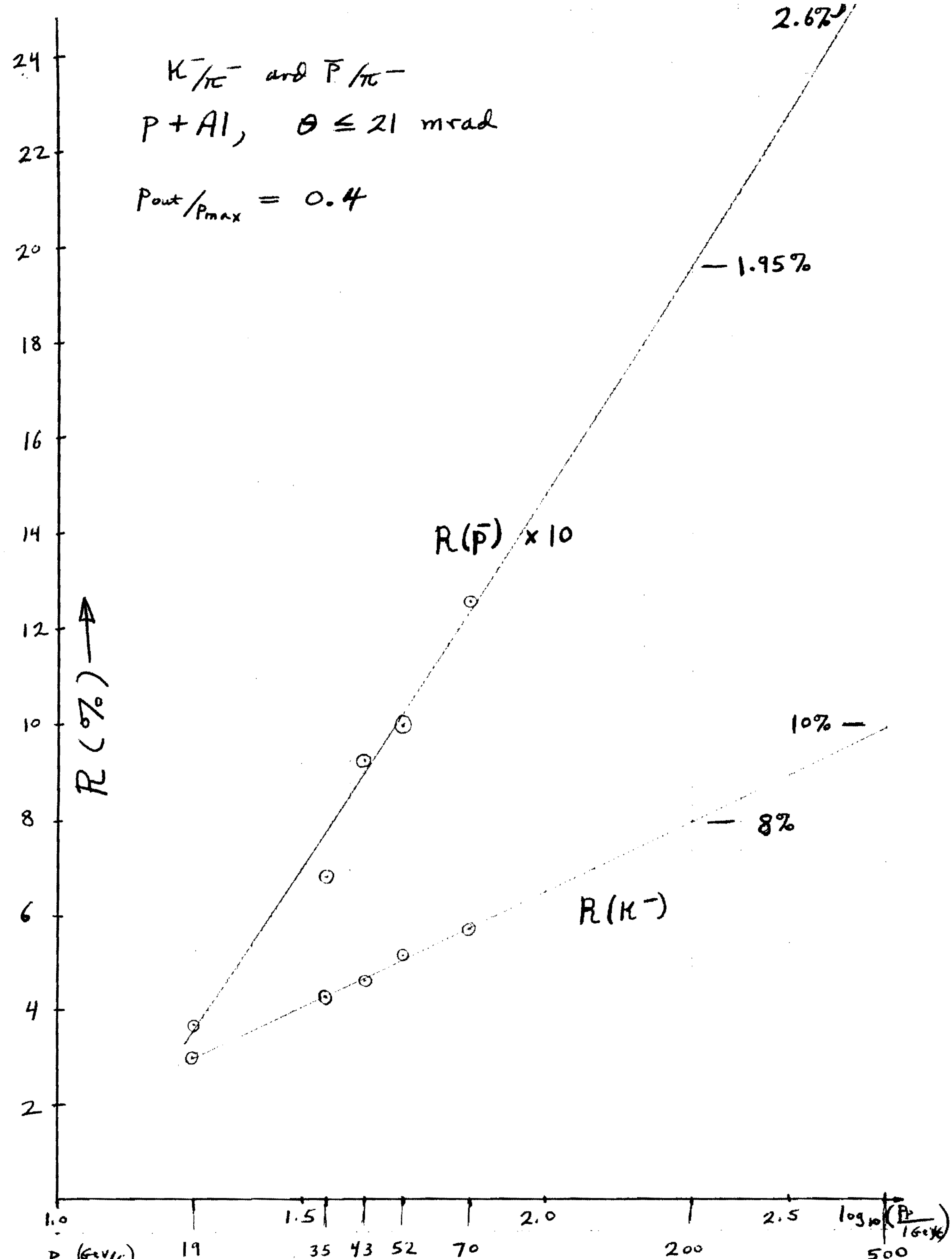

Appendix I, Figure 2

$(d^2\sigma_{K^-}/d\Omega dP)\,/\,(d^2\sigma_{\pi^-}/d\Omega dP)$ and analogous values for antiprotons ($R_{\bar{p}}$) and antideuterons ($P_{\bar{d}}$) are presented in table 1. Corrections, that take into account particle decay and their interaction with the matter in the beam path, were introduced into the measured values. Due to a very big length of the beam channel (≈ 120 m) the correction for kaon decay was $\approx 400\%$. In order to check whether this correction had been defined properly, the relative ammount of kaons in the beam was measured at two points at the end and in the middle of the beam, at a ≈ 80 m distance from the target. The values obtained for R_{K^-} coincided with an accuracy of 3% for $P = 10$ GeV/c and of 2% for $P = 13.3$ GeV/c.

As becomes obvious from table 1, the relative yield of heavy particles R from the Al target is somewhat heigher than from the Be target, however this difference is not very great. In the present paper the measurements were made at angles θ different from 0. As it was noted earlier [2-3] the relative yields R depend weakly on θ. So, at $P = 39$ GeV/c the ratio $R_{\bar{p}}$ increases by $(35 \pm 4)\%$ with the increase of the square transferred momentum $t \approx p^2\theta^2$ from 0 to 0.7 $(\mathrm{GeV}/c)^2$. If we approximate this dependence with the experimental $R_{\bar{p}}(t) \approx \exp(-at)$, and assume that it is valid in the region of small momenta P, then the difference between the relative antiproton yields at $\theta = 0$ and 47 mrad and $P = 13.3$ GeV/c will be 15%, and for $P = 10$ GeV/c and $\theta = 0$, $R_{\bar{p}}$ practically coincides with the value, measured at $\theta = 27$ mrad.

The measured values R are presented in fig. 1 together with the data, obtained at larger momenta [2, 3]. From this figure it can be seen, that the ratio $R_{\bar{p}}$ for small angles θ goes through the maximum $R_{\bar{p}\,max} = 3 \times 10^{-2}$ at $P = 13$ GeV/c.

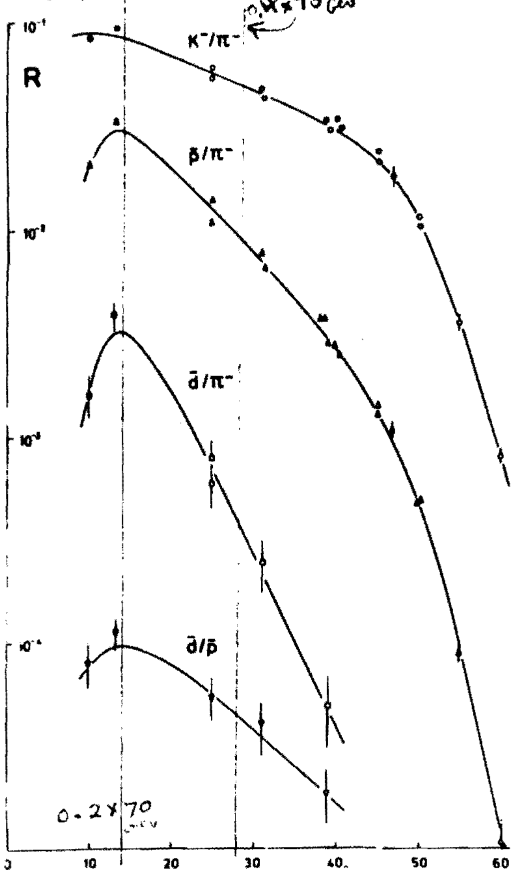

Fig. 1. Relative yields R of kaons, antiprotons and antideuterons, produced in p-Al and p-Be collisions at $E_0 = 70$ GeV. P equals the momentum of the secondaries. Dark pions are the results of the present paper, light points are the data [1-3]. The curves were drawn by hand.

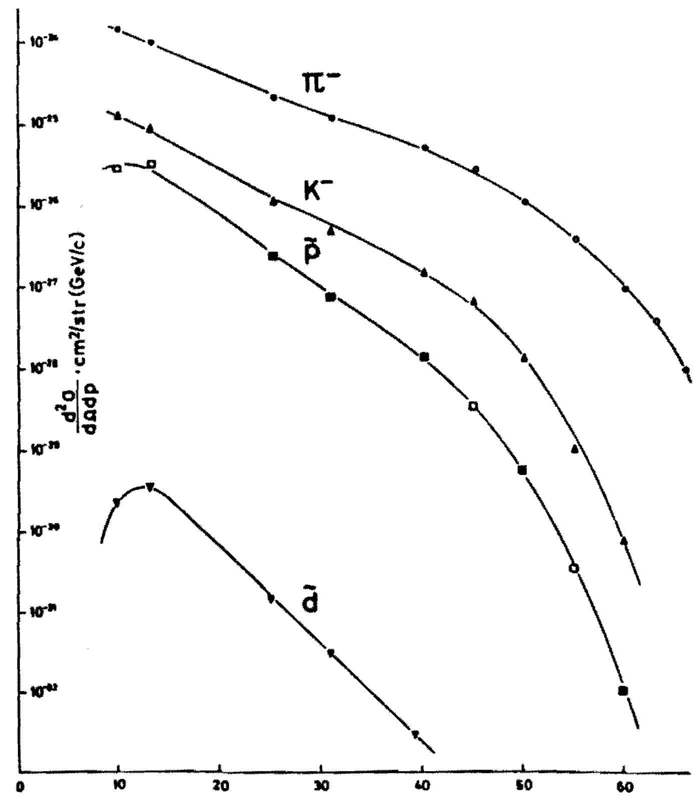

Fig. 2. Differential cross-sections for pion, kaon, antiproton and antideuteron production with momentum P in p-Al collisions at $E_0 = 70$ GeV. Dark points are cross-sections, measured at $\theta = 0^{\circ}$. Light points were obtained by cross-section extrapolation to $\theta = 0^{\circ}$ (see the tex The curves were drawn by hand.

FIGURE 3

APPENDIX I

Hadron Beams in the Neutrino Area.

J. W. Lamsa, V. E. Barnes and D. D. Carmony

Purdue University, March 22, 1971

The ratio of muons to pions $(\frac{\mu}{\pi})$ has been calculated for the hadron beams which will service the NAL 15 ft. bubble chamber and the ANL 30 inch bubble chamber. The source of muons is from the decay of pions in the hadron beam lines. We consider later an additional source of muons which would result if a hadron target is not used. The properties of these hadron beams are described by J. Lach and S. Pruss, National Accelerator Laboratory, TM-285 (1971).

The Monte Carlo beam program LLURCH by D. H. Stork, U.C.L.A. and J. L. Lloyd, Oxford, has been used to calculate the $\frac{\mu}{\pi}$ ratios. The positions, dimensions and fields of the beam elements set up in the program are those described in TM-285. LLURCH operates in the following way: particles are started from the hadron target and traced from element to element until they are lost from the beam or reach the end. A particle may be lost from the beam by striking a magnet or by decay. Scattering and losses in slits are also accounted for. For details see the LLURCH write-up.

The muons considered in calculating the $\frac{\mu}{\pi}$ ratio in the case of the 15 ft. chamber, are those which fall within a 12 ft. diameter circle on a plane perpendicular to the beam line at the position of the chamber. For the 30 inch chamber, which has a depth of 15 in., a 30 in. x 15 in. rectangle was used. The number of muons at the 15 ft. chamber includes those which strike a quadrupole after the last bend in the beam. Because of the angles and distance involved these muons also enter the bubble chamber. This procedure was not used for the beam to the 30 inch chamber since there are no elements after the last bend.

LLURCH was run both with and without magnetized slits. The slits, made of iron, were 10 ft. long with a field of 10 kG. The effect of the magnetized slits was to reduce the $\frac{\mu}{\pi}$ ratio by a factor of only 0.8 to 0.9. This was true for both beams and had little dependence on momentum. The effect of the greater bending power in the slits at lower momentum is compensated by the fact that at lower momentum more of the muons that get to the chamber come from decays occuring after the last bend in the beam (and after the slits).

The spacial distribution of the muons in the bubble chambers will be more dispersed than that of the pions which form a small image of the target. Approximately 1/3 of the muons in the 15 ft. chamber will overlap with the pion image of the target. For the 30 inch chamber the overlap is less than 5 percent. The $\frac{\mu}{\pi}$ ratio for all muons in the chamber has been calculated for both beams with unmagnetized slits at the following momenta: 30, 50, 100, 200, and 400 GeV/c. The results are presented in Fig. 1.

We now consider an additional source of muons which would result if the hadron target is not used and the source of pions is from the neutrino tunnel. Particles coming through an aperture in the shield will be steered over to the hadron beam. Pions decaying in the neutrino tunnel (1337 ft. long) create a spectrum (in momentum) of muons. For a given decay distance, the momentum spectrum of the pions will determine the momentum spectrum of the muons. The transformation can be made simply by using the fact that decay pions of energy E_o will yield a uniform energy spectrum of muons from 0.57 E_o to E_o. We will make the calculation for both 200 GeV/c and 500 GeV/c incident protons.

We have used the Hagedorn-Ranft calculation of forward production of negative pions as given in TM-285. The approximation that the average decay angle of a pion with a particular momentum is small compared with the width of the angular distribution of pions at that momentum is made. (The average pion decay angle is roughly $\frac{1}{10}$ the width of the production angular distributions.) Given the pion momentum distribution the muon momentum distribution is calculated. The muon spectrum is normalized according to the probability for pion decay in neutrino tunnel and the pion spectrum according to decay in the entire beam length, neutrino target to bubble chamber. We have normalized for pion decay only in the neutrino tunnel rather than all the way up to the first momentum slit because studies with LLURCH showed that a negligible number of muons would reach the bubble chambers from pion decays in the region from the end of the tunnel to the first slit. The pion and muon spectra yield directly for any momentum the $\frac{\mu}{\pi}$ ratio (for muons produced in the tunnel) in the bubble chamber for the same momentum bite of both particles. The results are shown in Fig. 2. Because the slits are somewhat transparent to muons the beam will transmit a larger equivalent momentum bite for muons. This effect, however, turns out to be negligible at momenta less than 100 GeV/c, only at 400 GeV/c would it as much as double the number of muons predicted and here the number is very small anyway. Without the use of a hadron target the $\frac{\mu}{\pi}$ ratio in the bubble chamber will be the sum of ratios from Figs. 1 and 2. Unlike the muons which result from pion decay in the hadron beam lines, the muons coming from the neutrino tunnel will focus to an image of the target just as do the pions.

We wish to thank S. Pruss for the several useful suggestions concerning this work.

MUONS FROM PION DECAYS IN THE HADRON BEAM LINES

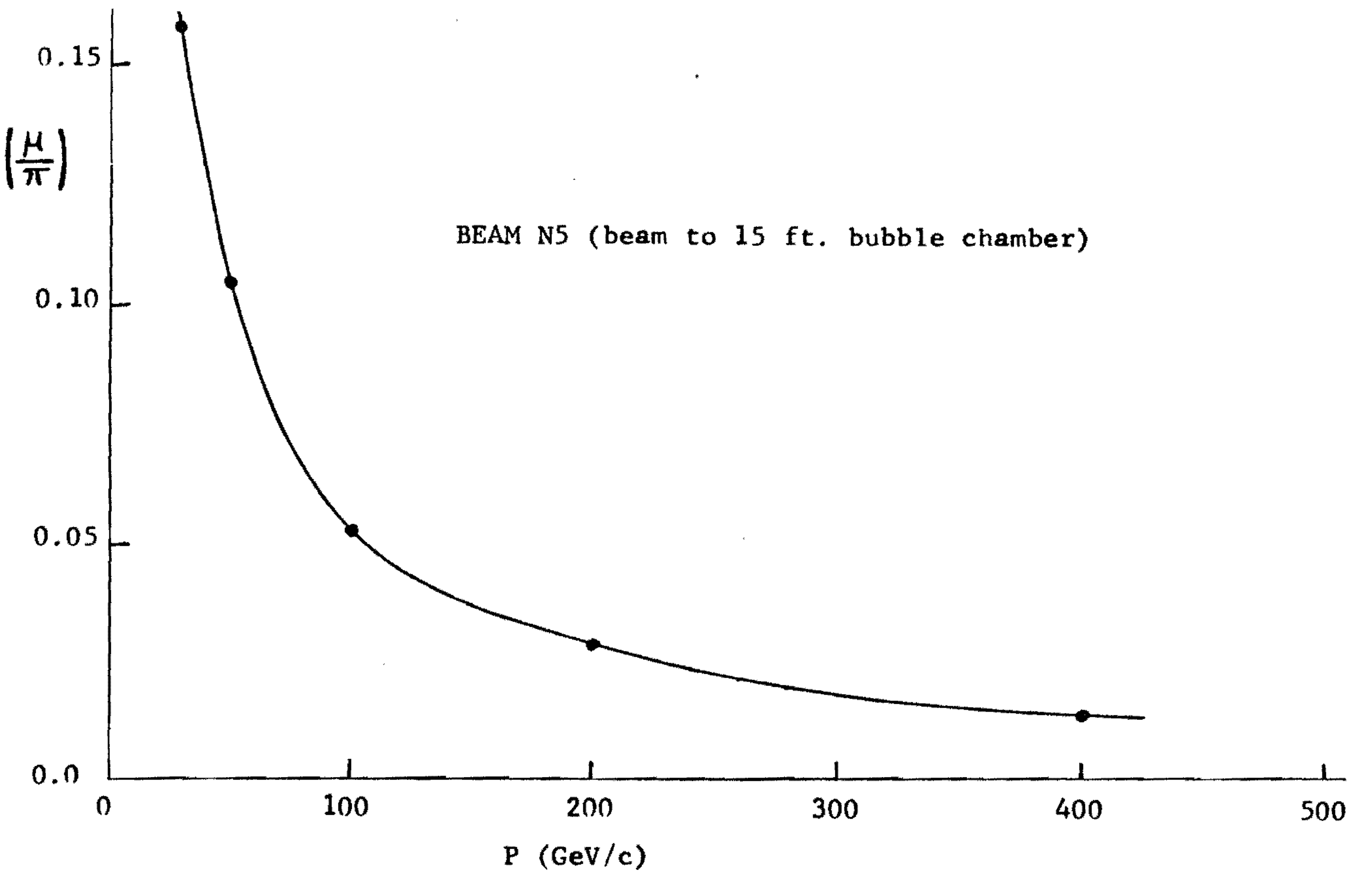

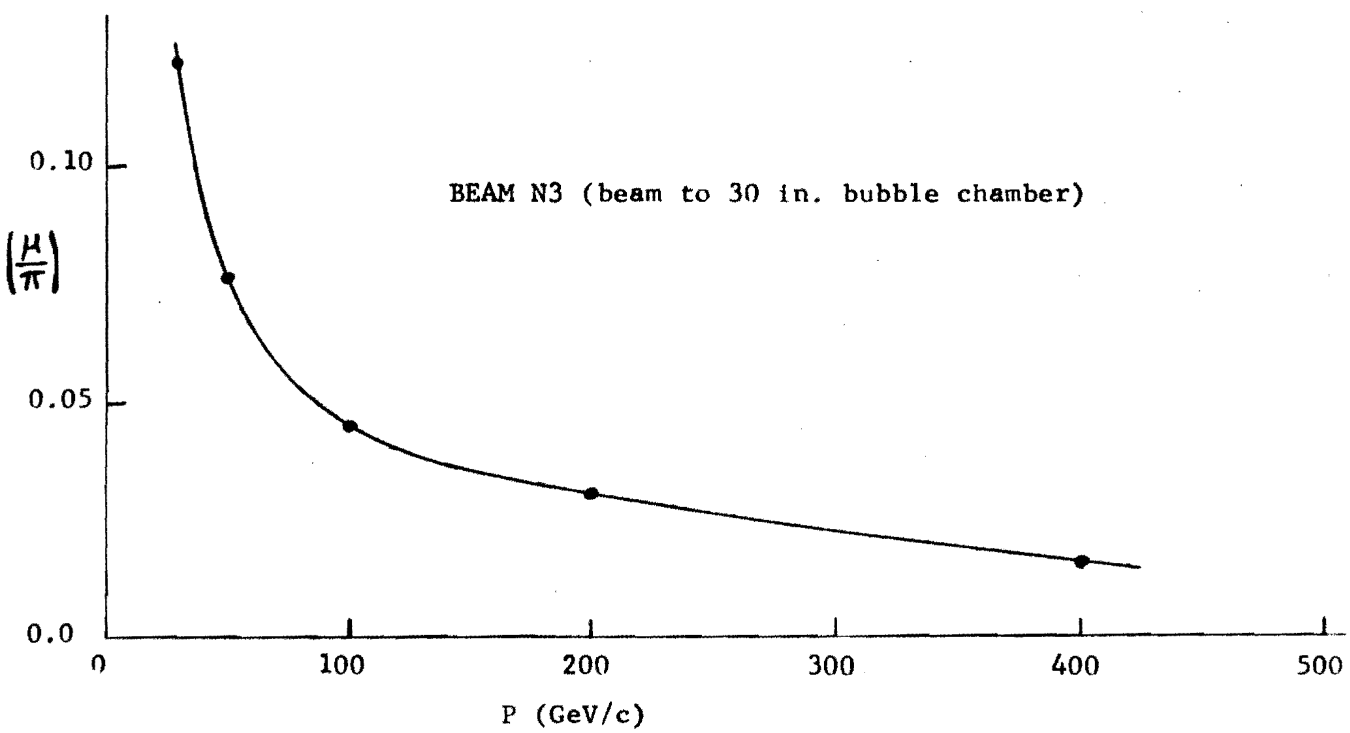

FIG. 1

MUONS FROM PION DECAYS IN THE NEUTRINO TUNNEL

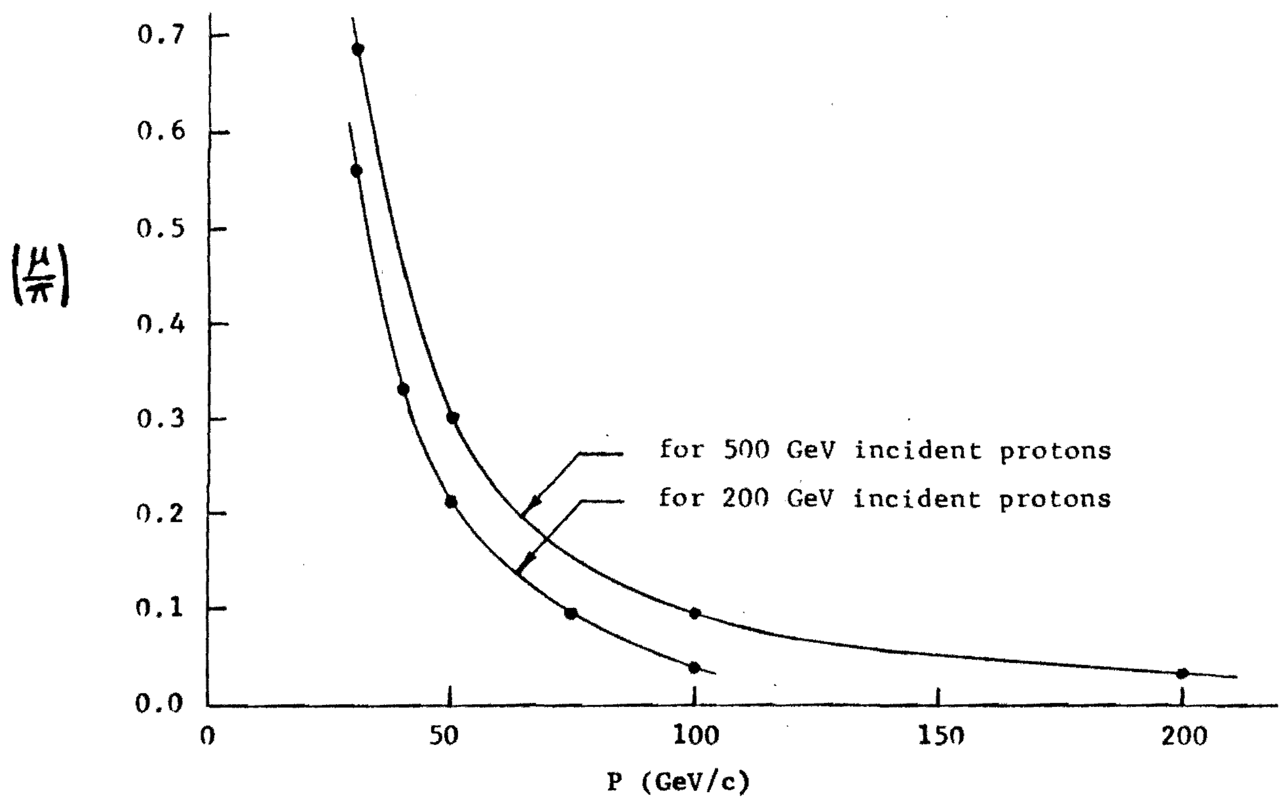

FIG. 2